Backscattering in antiresonant hollow-core fibers: over 40 dB lower than in standard optical fibers

V. Michaud-Belleau[1], E. Numkam Fokoua[2], T. D. Bradley[2], J. R. Hayes[2], Y. Chen[2], F. Poletti[2], D. J. Richardson[2], J. Genest[1], and R. Slavík[2,*]

[1] Centre d'optique, photonique et laser, Université Laval, Québec, QC, G1V 0A6, Canada
[2] Optoelectronics Research Centre, University of Southampton, Southampton, SO17 1BJ, UK
[*] Corresponding author: r.slavik@soton.ac.uk

Compiled January 4, 2021

The elastic backscattering of light in optical fiber is a fundamental phenomenon which sets the ultimate performance of several fiber systems such as gyroscopes and bidirectional transfer links. Until now, efforts to reduce the backscattering coefficient have yielded limited results, with the lowest value sitting at around −76 dB/m in Ge-free silica core fiber at 1.55 µm. Here, we present what we believe to be the first measurement of backscattering from a low-loss antiresonant hollow-core fiber and show that it is more than 40 dB below reported values in silica-core fiber and hollow-core photonic bandgap fiber. The record-low level of −118 dB/m measured with our custom-built optical frequency-domain reflectometer is in good agreement with simulations in which we assume the scattering to originate from the intrinsic surface roughness. Our demonstration also shows that a tailored instrument can localize and quantify weak faults within a hollow-core fiber, enabling its detailed characterization.

http://dx.doi.org/10.1364/optica.XX.XXXXXX

The elastic scattering of light is the prime contributor to the transmission loss of state-of-the-art single-mode fiber (SMF) in the near-infrared and visible regions [1, 2]. Such scattering is not only undesirable because it leads to loss, but also because a fraction of the scattered light is inevitably recaptured by the fiber and guided backwards. This backscattered light is equivalent to a large number of delayed replicas of the forward-propagating signal that act as a source of noise whenever they are allowed to reach the detector, most critically when they can coherently mix with the signal [3]. This is especially problematic in systems relying on bidirectional propagation such as fiber optic gyroscopes [4], remote fiber sensors probed in reflection [5], and bidirectional fiber links used for either time and frequency transfer [3], telecommunications [6], or quantum key distribution [7], though the performance of unidirectional systems like optoelectronic oscillators can also be limited by double backscattered light that propagates with the signal [8]. Yet, backscattering can also be beneficial in certain instances, for example for distributed fiber sensing [9] or to find faults within deployed fibers [10].

Lowering the backscattering coefficient (BSC) of a standard SMF requires the diminution of either the recapture fraction η or the scattering loss α_s (BSC $= \eta\alpha_s$). The recapture fraction is determined by the acceptance angle, inversely proportional to mode field area in SMF [11], and thus can only be modestly lowered before bending loss becomes problematic. Loss caused by Rayleigh scattering in SMF, on the other hand, correlates with the fictive temperature, a parameter quantifying the disorder of the glass network which is typically higher in fiber than in bulk [12]. Techniques to lower this temperature have been employed in the ongoing quest to minimize the transmission loss of long-haul submarine systems [1]. In the Ge-free SMFs used therein, the scattering loss is the dominant contributor to the total loss and it lies at approximately 0.1 dB/km ($\alpha_s = 2.3\times10^{-5}$ m^{-1}). This is associated with a BSC of −76 dB/m assuming $\eta = 1.2\times10^{-3}$, about 4 dB below what is usually quoted for SMF at 1.55 µm [13]. However, further significant reduction of α_s is unlikely since the gap in fictive temperature between fiber and bulk is now mostly closed [1, 12]. Therefore, to go beyond the limits imposed by fundamental Rayleigh scattering in SMF, light should be guided in a less scattering medium.

After its initial demonstration some 20 years ago [14], the hollow-core photonic bandgap fiber (HC-PBGF) was thus considered a promising candidate to attain lower BSC. In such fibers, the overlap of the mode field with the glass microstructure is typically 0.1 to 1% [15] which, given similar acceptance angles, should lead at least to a commensurate 20 to 30 dB reduction in volumetric Rayleigh backscattering when compared to standard SMF [16]. However, reported measurements in commercial 7-cell HC-PBGFs have shown a BSC of −60 dB/m or higher [13, 17, 18].

Such unexpectedly high BSC has been tentatively attributed to surface scattering from glass interfaces, which in those early fibers may have been oscillating along the entire length [19]. In addition, even for perfectly straight glass membranes, air-glass surfaces display intrinsic roughness which cause scattering. This is due to frozen-in surface capillary waves (SCW) that are excited by fundamental thermal noise, and are believed to set the ultimate performance limits in terms of loss and BSC [20].

In recent years, another class of hollow-core fiber (HCF), the antiresonant fiber, has been at the focus of intense research. This is due in part to the promise of reduced surface scattering loss associated with the operation of the glass membranes at antiresonance [21]. In particular, the nested antiresonant nodeless fiber (NANF) geometry fulfills this promise and currently holds the record for the lowest loss in a HCF, 0.28 dB/km [22]. The demonstration in [22] also confirms the theoretical prediction of a scattering loss below 0.1 dB/km in NANF (below the value in SMF) [21]. Although such low scattering loss implies commensurately weak backscattering, BSC characterization of NANF has not been reported so far, to our knowledge. We speculate this is because commercial instruments are not designed to measure BSCs that are orders of magnitude below that of SMF.

In this Letter, we present the first range-resolved characterization of backscattering in an antiresonant HCF, revealing a BSC of −118 dB/m which is more than 40 dB lower than that of SMF. Below, we briefly present the NANF sample as well as the custom instrument designed to measure its BSC, discuss how the results compare with the predictions of a theoretical model based on surface roughness scattering, and describe a series of tests performed to confirm the soundness of our data analysis.

For this demonstration, a 219-m sample of NANF manufactured at the University of Southampton was used. Short SMF-28 pigtails (≈ 24 cm) with angled physical contact connectors were spliced at both extremities of the spooled sample to facilitate its interfacing with characterization instruments and to seal its hollow core so as to prevent degradation. For each splice, a (250±20) µm segment of graded-index multimode fiber was used as a mode-field adapter to decrease the loss per interconnection, which we estimated at (1.6±0.2) dB. The loss of the NANF itself was measured via cutback to be 1.2 dB/km at 1.55 µm, higher than the current record based on an improved version of a similar design [22] but not problematic for the purposes of backscattering characterization. The total transmission loss of the pigtailed sample exposed to the laboratory environment was found to slowly fluctuate between 3.1 and 3.7 dB, a phenomenon that we attribute to the formation of a resonant cavity between the two air-glass splices (≈ 3.6% Fresnel reflections). We did not attempt to weaken these reflections, but this could eventually be achieved using improved interconnection techniques [23].

To perform the range-resolved backscattering measurement, we built an optical frequency-domain reflectometer (OFDR) optimized for sensitivity and dynamic range at the expense of versatility and spatial resolution (Fig. 1). The core of the instrument is a self-heterodyne Mach-Zehnder interferometer ("measurement interferometer") with a 27 MHz frequency shift produced through an acousto-optic modulator (AOM). A low-phase-noise and periodically chirped laser signal at 1539.8 nm, with a full sweep bandwidth $\Delta f = 335$ MHz and average chirp rate $\gamma = 93.5$ GHz/s, is used to illuminate the measurement interferometer as well as a reference interferometer. The purpose of this second interferometer (100-m polarization-maintaining SMF) is to track the chirp's deviation from linearity in order to preserve the resolution through post-processing correction [24]. To this

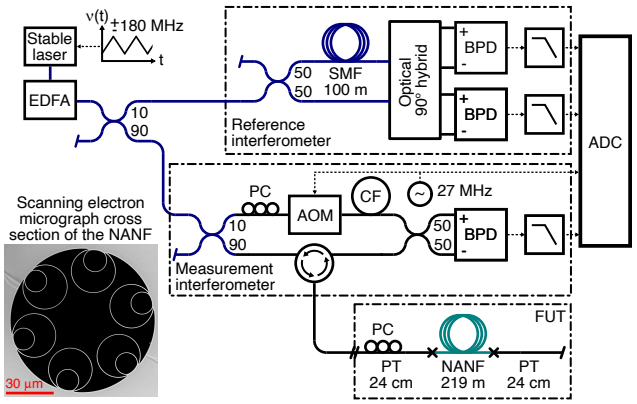

Fig. 1. Layout of the coherent OFDR operating at 1539.8 nm. EDFA, erbium-doped fiber amplifier; PC, polarization controller; AOM, acousto-optic modulator; CF, compensation fiber; BPD, balanced photodetector; ADC, analog-to-digital converter (digitizer); PT, pigtail; FUT, fiber under test. Solid lines represent fibers (black is standard, blue is polarization maintaining) and dashed lines represent electrical cables.

effect, the signal produced by the three balanced photodetectors, together with the signal driving the AOM, are simultaneously digitized at 125 MS/s for 0.8 s and processed offline. Since the reference interferometer is not used to trigger the digitizer, the measurement range is determined by the sampling rate and reaches 100 km (ignoring the effects of fiber attenuation), one order of magnitude below the laser's nominal coherence length.

In order to maintain a high dynamic range in spite of the strong reflections caused by the air-glass splices, a Kaiser window with $\beta = 12$ is employed to compute the spectra. This choice yields an effective spatial resolution of $cN/(2\Delta f) = 0.9$ m in vacuum, where c is the speed of light and $N = 2$ is the window's equivalent noise bandwidth (measured in spectral bins). Moreover, the contribution of the remote splice at 219 m is carefully suppressed through polarization control to avoid the burying of the signal of interest by the associated phase noise lobes [25]. The disadvantage of this approach is that it precludes the use of polarization diversity detection. However, it is one of the key features that enable an outstanding sensitivity of −127 dB/m in a single laser sweep, a value determined in equal parts by digitizer noise and shot noise. For a stationary scattering signal, this sensitivity can be improved by averaging sweeps before computing the spectrum [10]. More information about the instrument and fiber can be found in Supplement 1.

Figure 2 compares the reflectance density measured for NANF with that of a standard SMF-28 sample characterized with the same instrument. Both curves are calibrated to compensate for the insertion loss of the output coupler, circulator, and interconnections, thus showing the intrinsic backscattering of the fibers. Moreover, since OFDR relies on coherent detection, both curves correspond to the projection along a single polarization and are thus approximately 3 dB lower than the total reflectance density usually measured with an incoherent optical time domain reflectometer or an OFDR based on polarization diversity detection. For this figure, 5 sweeps were averaged to compute each normalized power spectral density (PSD), yielding an effective noise floor of $-127 - 10\log_{10}(5) = -134$ dB/m. The 200/5 = 40 resulting PSDs were then averaged to decrease the spectral variance. The displayed curves persist with such

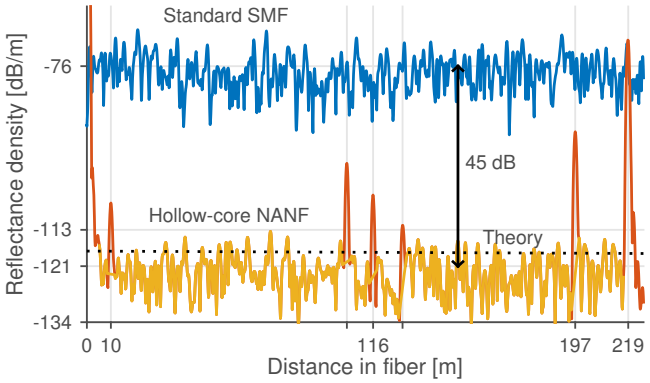

Fig. 2. Measured reflectance density (single-polarization, 0.9 m resolution) in NANF versus in SMF. The yellow trace excludes the peaks attributed to localized defects, the dotted black line constitutes the theoretical prediction of −118 dB/m.

spectral averaging, becoming better defined, and are also repeatable over several minutes. Their uneven appearance is not due to measurement noise: it can be explained by a combination of fading noise and polarization effects in the samples [10].

For the NANF, the large peaks at 0 m and 219 m are caused by the Fresnel reflections at the points where the fiber is spliced to the SMF pigtails. The polarization-suppressed peak at 219 m reaches a level comparable to the backscattering in SMF, which constitutes the practical suppression limit for this pigtailed sample. Between the splices, the NANF's reflectance density is −113 dB/m on average. However, this average is calculated by including the intermediate peaks that rise significantly above the apparent backscattering level at 10 m, 197 m, and around 116 m. As demonstrated below, these peaks consistently appear in the data and are thus attributed to localized inhomogeneities in the NANF. Without these peaks, the average reflectance density becomes −121 dB/m (yellow trace). We therefore estimate that the intrinsic total BSC of the NANF is −121+3 = −118 dB/m.

To explain such a low BSC, the contributions of inhomogeneities within the glass microstructure, within the air that fills the core, and at the air-glass interfaces need to be carefully considered. First, since the NANF's acceptance angle is very small ($\theta \approx 0.03$) and the fraction of power ξ guided in glass below 10^{-4}, the contribution of volumetric Rayleigh backscattering from silica, which is proportional to $\theta^2\xi$, is more than 55 dB lower than in SMF and can thus be neglected here [16]. Second, while the scattering loss in air close to atmospheric pressure is only 20 to 25 dB smaller than that in SMF [26], it plays no measurable role here since the thermal Doppler broadening at room temperature ($\approx$ 500 MHz) is orders of magnitude larger than the 300 kHz measurement bandwidth. In a general context, the NANF could be evacuated to reduce the air contribution below the fundamental backscattering level measured here. This leaves surface scattering whose contribution we predict from coupled mode theory [27] and the surface roughness statistics (the full details of the theoretical model developed for this analysis fall outside the scope of this short Letter and will thus be reported elsewhere). Based on the geometry of the NANF sample used here and on the fundamental SCW roughness measured in HC-PBGFs [20] (unfortunately, data about roughness in NANF is not available yet), our simulations predict a BSC of −115 dB/m, or −118 dB/m when measured along a single polarization, 3 dB above the value here. We consider this to constitute a reasonable agreement, supporting the conclusion that backscattering in NANF finds its origin in intrinsic surface roughness. Using the same approach with the 7-cell PBGF geometry cited above yields a BSC of −77 dB/m, approximately 40 dB higher than in NANF. This agrees with a roughly 100x larger overlap of the mode field with the interfaces (the BSC being proportional to the square of this quantity). The discrepancy between measured and modeled backscattering levels in those commercial HC-PBGFs has been noted before and assigned speculatively to the fact that the roughness on their thin glass walls (< 100 nm) may be stronger than that resulting from frozen-in SCW alone [19].

Figure 3 depicts the outcomes of tests that we conducted to verify the validity of our data interpretation. In (a), the sweep's repetition rate was varied to increase the chirp rate γ without changing the spatial resolution. In the frequency domain, such modification has the effect of spreading the scattering signal over a larger bandwidth, thus inducing a relative shift with noises that originate from the instrument. The consistent spectral structure indicates that additive, phase, and intensity noises are weaker than the scattering signal over the extent of the NANF (0 m to 219 m). In (b), the data used for Fig. 2 was averaged in different manners, trading between temporal and spectral (PSD) averaging. The lowest points of the trace follow the predicted measurement noise floor (dotted lines at −127, −134, and −141 dB/m) over most of the scattering region and their level decreases with higher temporal averaging, confirming the general validity of the additive noise model. Meanwhile, the highest points of the traces stay at a constant level, establishing that the backscattering signal is repeatable as expected for scattering caused by static surface roughness. Finally, in (c), the NANF sample was illuminated from the opposite direction and the measured reflectance density was flipped in post-processing to show distance from the same splice. Although imperfect because of the movement of the pigtails and modified polarization launch conditions, there is reasonable agreement between the two traces. This corroborates our interpretation that the intermediate peaks are caused by localized faults and not by noise.

In conclusion, we measured the reflectance density of a nested antiresonant nodeless fiber with a 0.9 m resolution and up to −138 dB/m sensitivity and found its intrinsic backscattering coefficient to be −118 dB/m. This unprecedented value, more than 40 dB below reported figures in standard SMFs and HC-PBGFs, is likely limited by scattering from the thermally-driven surface roughness of the microstructure. Together with the low transmission loss now approaching that of standard SMF [22], the polarization purity [28], and other desirable features inherent to all hollow-core fibers (low thermal sensitivity, non-linearity, magnetic susceptibility, etc. [15]), this should allow NANFs to set new performance benchmarks in applications today limited by backscattering. As a specific example, using a NANF with low-back-reflection interconnections [23] is expected to provide a significant reduction (> 40 dB in theory) of the backscattering-limited noise and bias drift in fiber-optic gyroscopes (FOGs) driven by highly-coherent lasers [4]. In addition to the reduced Kerr and Shupe effects already demonstrated in HCF-based FOGs, this could enable the improvement of the scale factor stability required for the inertial navigation of aircrafts [13]. Finally, our demonstration reveals that the partial characterization of a low-loss HCF is possible with only access to a single fiber end. Monitoring the distributed and localized inhomogeneities that backscatter light can provide the precious information required to improve NANF's fabrication and thus further reduce its loss, potentially below that of the best SMF.

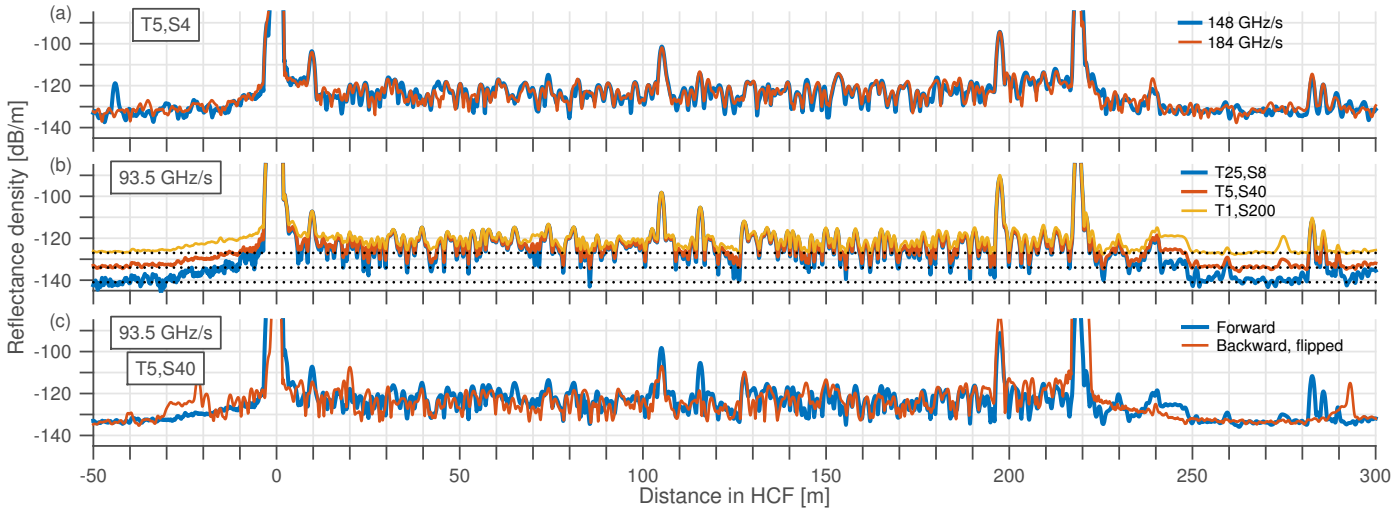

Fig. 3. Measured reflectance density in NANF. (a) Different chirp rates with 5 temporal averages, 4 spectral averages (T5,S4). (b) Different trades between temporal and spectral averaging for a chirp rate of 93.5 GHz/s. The dotted lines represent the predicted measurement noise floors. (c) Forward versus backward illumination, rectified to show distance from the same splice.

See Supplement 1 for supporting content.

FUNDING

Engineering and Physical Sciences Research Council ("Air-guide Photonics", EP/P030181/1); European Research Council (682724); Fonds de recherche du Québec – Nature et technologies; Natural Sciences and Engineering Research Council of Canada.

ACKNOWLEDGMENTS

E.N.F. and R.S. acknowledge support of RAEng research and senior fellowships. The data for this work is accessible through the University of Southampton Institutional Research Repository (DOI: 10.5258/SOTON/xxxxx).

DISCLOSURES

The authors declare no conflicts of interest.

REFERENCES

1. Y. Tamura, H. Sakuma, K. Morita, M. Suzuki, Y. Yamamoto, K. Shimada, Y. Honma, K. Sohma, T. Fujii, and T. Hasegawa, J. Light. Technol. **36**, 44 (2018).
2. R. Olshansky, Rev. Mod. Phys. **51**, 341 (1979).
3. Ł. Śliwczyński, P. Krehlik, and M. Lipiński, Meas. Sci. Technol. **21**, 075302 (2010).
4. S. W. Lloyd, M. J. Digonnet, and S. Fan, J. Light. Technol. **31**, 2070 (2013).
5. J. H. Chow, I. C. M. Littler, D. E. McClelland, and M. B. Gray, Opt. Express **14**, 4617 (2006).
6. J. Xu, M. Li, and L.-K. Chen, J. Light. Technol. **29**, 3632 (2011).
7. D. Subacius, A. Zavriyev, and A. Trifonov, Appl. Phys. Lett. **86**, 011103 (2005).
8. J. P. Cahill, W. Zhou, and C. R. Menyuk, Appl. Opt. **56**, B18 (2017).
9. L. Palmieri and L. Schenato, The Open Opt. J. **7** (2013).
10. J. P. Von Der Weid, R. Passy, G. Mussi, and N. Gisin, J. Light. Technol. **15**, 1131 (1997).
11. D. L. Philen, I. A. White, J. F. Kuhl, and S. C. Mettler, IEEE Transactions on Microw. Theory Tech. **30**, 1487 (1982).
12. S. Sakaguchi and S.-i. Todoroki, Appl. Opt. **37**, 7708 (1998).
13. S. W. Lloyd, V. Dangui, M. J. F. Digonnet, S. Fan, and G. Kino, Opt. Lett. **35**, 121 (2010).
14. R. F. Cregan, B. J. Mangan, J. C. Knight, T. A. Birks, P. St. J. Russell, P. J. Roberts, and D. C. Allan, Science. **285**, 1537 (1999).
15. F. Poletti, M. N. Petrovich, and D. J. Richardson, Nanophotonics. **2**, 315 (2013).
16. M. Nakazawa, J. Opt. Soc. Am. **73**, 1175 (1983).
17. M. Wegmuller, M. Legré, N. Gisin, T. P. Hansen, C. Jakobsen, and J. Broeng, Opt. Express **13**, 1457 (2005).
18. X. Xu, M. Yan, N. Song, C. Wu, F. Teng, and J. Jin, IEEE Photonics Technol. Lett. **28**, 2858 (2016).
19. V. Dangui, M. J. Digonnet, and G. S. Kino, J. Light. Technol. **27**, 3783 (2009).
20. P. J. Roberts, F. Couny, H. Sabert, B. J. Mangan, D. P. Williams, L. Farr, M. W. Mason, A. Tomlinson, T. A. Birks, J. C. Knight, and P. St. J. Russell, Opt. Express **13**, 236 (2005).
21. F. Poletti, Opt. Express **22**, 23807 (2014).
22. G. T. Jasion, T. D. Bradley, K. Harrington, H. Sakr, Y. Chen, E. N. Fokoua, I. A. Davidson, A. Taranta, J. R. Hayes, D. J. Richardson, and F. Poletti, "Hollow core NANF with 0.28 dB/km attenuation in the C and L bands," in *Optical Fiber Communication Conference*, (Optical Society of America, 2020), pp. Th4B–4.
23. M. Komanec, D. Suslov, S. Zvanovec, Y. Chen, T. Bradley, S. R. Sandoghchi, E. N. Fokoua, G. Jasion, M. Petrovich, F. Poletti, D. J. Richardson, and R. Slavík, IEEE Photonics Technol. Lett. **31**, 723 (2019).
24. T.-J. Ahn, J. Y. Lee, and D. Y. Kim, Appl. Opt. **44**, 7630 (2005).
25. S. Venkatesh and W. V. Sorin, J. Light. Technol. **11**, 1694 (1993).
26. A. Bucholtz, Appl. Opt. **34**, 2765 (1995).
27. D. Marcuse, *Theory of dielectric optical waveguides* (Elsevier, 2013).
28. A. Taranta, E. N. Fokoua, S. A. Mousavi, J. Hayes, T. Bradley, G. Jasion, and F. Poletti, Nat. Photonics pp. 1–7 (2020).

FULL REFERENCES

1. Y. Tamura, H. Sakuma, K. Morita, M. Suzuki, Y. Yamamoto, K. Shimada, Y. Honma, K. Sohma, T. Fujii, and T. Hasegawa, "The first 0.14-db/km loss optical fiber and its impact on submarine transmission," J. Light. Technol. **36**, 44–49 (2018).
2. R. Olshansky, "Propagation in glass optical waveguides," Rev. Mod. Phys. **51**, 341 (1979).
3. Ł. Śliwczyński, P. Krehlik, and M. Lipiński, "Optical fibers in time and frequency transfer," Meas. Sci. Technol. **21**, 075302 (2010).
4. S. W. Lloyd, M. J. Digonnet, and S. Fan, "Modeling coherent backscattering errors in fiber optic gyroscopes for sources of arbitrary line width," J. Light. Technol. **31**, 2070–2078 (2013).
5. J. H. Chow, I. C. M. Littler, D. E. McClelland, and M. B. Gray, "Laser frequency-noise-limited ultrahigh resolution remote fiber sensing," Opt. Express **14**, 4617–4624 (2006).
6. J. Xu, M. Li, and L.-K. Chen, "Rayleigh noise reduction in 10-gb/s carrier-distributed wdm-pons using in-band optical filtering," J. Light. Technol. **29**, 3632–3639 (2011).
7. D. Subacius, A. Zavriyev, and A. Trifonov, "Backscattering limitation for fiber-optic quantum key distribution systems," Appl. Phys. Lett. **86**, 011103 (2005).
8. J. P. Cahill, W. Zhou, and C. R. Menyuk, "Additive phase noise of fiber-optic links used in photonic microwave-generation systems," Appl. Opt. **56**, B18–B25 (2017).
9. L. Palmieri and L. Schenato, "Distributed optical fiber sensing based on rayleigh scattering," The Open Opt. J. **7** (2013).
10. J. P. Von Der Weid, R. Passy, G. Mussi, and N. Gisin, "On the characterization of optical fiber network components with optical frequency domain reflectometry," J. Light. Technol. **15**, 1131–1141 (1997).
11. D. L. Philen, I. A. White, J. F. Kuhl, and S. C. Mettler, "Single-mode fiber otdr: Experiment and theory," IEEE Transactions on Microw. Theory Tech. **30**, 1487–1496 (1982).
12. S. Sakaguchi and S.-i. Todoroki, "Rayleigh scattering of silica core optical fiber after heat treatment," Appl. Opt. **37**, 7708–7711 (1998).
13. S. W. Lloyd, V. Dangui, M. J. F. Digonnet, S. Fan, and G. Kino, "Measurement of reduced backscattering noise in laser-driven fiber optic gyroscopes," Opt. Lett. **35**, 121–123 (2010).
14. R. F. Cregan, B. J. Mangan, J. C. Knight, T. A. Birks, P. St. J. Russell, P. J. Roberts, and D. C. Allan, "Single-mode photonic band gap guidance of light in air," Science. **285**, 1537–1539 (1999).
15. F. Poletti, M. N. Petrovich, and D. J. Richardson, "Hollow-core photonic bandgap fibers: technology and applications," Nanophotonics. **2**, 315–340 (2013).
16. M. Nakazawa, "Rayleigh backscattering theory for single-mode optical fibers," J. Opt. Soc. Am. **73**, 1175–1180 (1983).
17. M. Wegmuller, M. Legré, N. Gisin, T. P. Hansen, C. Jakobsen, and J. Broeng, "Experimental investigation of the polarization properties of a hollow core photonic bandgap fiber for 1550 nm," Opt. Express **13**, 1457–1467 (2005).
18. X. Xu, M. Yan, N. Song, C. Wu, F. Teng, and J. Jin, "Measurement of backscattering in hollow core photonic bandgap fiber based on mach–zehnder and michelson hybrid interferometer," IEEE Photonics Technol. Lett. **28**, 2858–2861 (2016).
19. V. Dangui, M. J. Digonnet, and G. S. Kino, "Modeling of the propagation loss and backscattering in air-core photonic-bandgap fibers," J. Light. Technol. **27**, 3783–3789 (2009).
20. P. J. Roberts, F. Couny, H. Sabert, B. J. Mangan, D. P. Williams, L. Farr, M. W. Mason, A. Tomlinson, T. A. Birks, J. C. Knight, and P. St. J. Russell, "Ultimate low loss of hollow-core photonic crystal fibres," Opt. Express **13**, 236–244 (2005).
21. F. Poletti, "Nested antiresonant nodeless hollow core fiber," Opt. Express **22**, 23807–23828 (2014).
22. G. T. Jasion, T. D. Bradley, K. Harrington, H. Sakr, Y. Chen, E. N. Fokoua, I. A. Davidson, A. Taranta, J. R. Hayes, D. J. Richardson, and F. Poletti, "Hollow core NANF with 0.28 dB/km attenuation in the C and L bands," in *Optical Fiber Communication Conference,* (Optical Society of America, 2020), pp. Th4B–4.
23. M. Komanec, D. Suslov, S. Zvanovec, Y. Chen, T. Bradley, S. R. Sandoghchi, E. N. Fokoua, G. Jasion, M. Petrovich, F. Poletti, D. J. Richardson, and R. Slavík, "Low-loss and low-back-reflection hollow-core to standard fiber interconnection," IEEE Photonics Technol. Lett. **31**, 723–726 (2019).
24. T.-J. Ahn, J. Y. Lee, and D. Y. Kim, "Suppression of nonlinear frequency sweep in an optical frequency-domain reflectometer by use of hilbert transformation," Appl. Opt. **44**, 7630–7634 (2005).
25. S. Venkatesh and W. V. Sorin, "Phase noise considerations in coherent optical fmcw reflectometry," J. Light. Technol. **11**, 1694–1700 (1993).
26. A. Bucholtz, "Rayleigh-scattering calculations for the terrestrial atmosphere," Appl. Opt. **34**, 2765–2773 (1995).
27. D. Marcuse, *Theory of dielectric optical waveguides* (Elsevier, 2013).
28. A. Taranta, E. N. Fokoua, S. A. Mousavi, J. Hayes, T. Bradley, G. Jasion, and F. Poletti, "Exceptional polarization purity in antiresonant hollow-core optical fibres," Nat. Photonics pp. 1–7 (2020).